The Accuracy of Determining Three-Dimensional Radiative Transfer Effects in Cumulus Clouds Using Ground-Based Profiling Instruments

ROBERT PINCUS AND CÉCILE HANNAY*

NOAA–CIRES Climate Diagnostics Center, Boulder, Colorado

K. FRANKLIN EVANS

Program in Atmospheric and Oceanic Science, University of Colorado, Boulder, Colorado

(Manuscript received 5 August 2004, in final form 14 October 2004)

ABSTRACT

Three-dimensional radiative transfer calculations are accurate, though computationally expensive, if the spatial distribution of cloud properties is known. The difference between these calculations and those using the much less expensive independent column approximation is called the 3D radiative transfer effect. Assessing the magnitude of this effect in the real atmosphere requires that many realistic cloud fields be obtained, and profiling instruments such as ground-based radars may provide the best long-term observations of cloud structure. Cloud morphology can be inferred from a time series of vertical profiles obtained from profilers by converting time to horizontal distance with an advection velocity, although this restricts variability to two dimensions. This paper assesses the accuracy of estimates of the 3D effect in shallow cumulus clouds when cloud structure is inferred in this way. Large-eddy simulations provide full three-dimensional, time-evolving cloud fields, which are sampled every 10 s to provide a "radar's eye view" of the same cloud fields. The 3D effect for shortwave surface fluxes is computed for both sets of fields using a broadband Monte Carlo radiative transfer model, and intermediate calculations are made to identify reasons why estimates of the 3D effect differ in these fields. The magnitude of the 3D effect is systematically underestimated in the two-dimensional cloud fields because there are fewer cloud edges that cause the effect, while the random error in hourly estimates is driven by the limited sample observed by the profiling instrument.

1. Three-dimensional radiative transfer effects and why one might estimate them in two-dimensional clouds

The physics that underlies radiative transfer in the atmosphere is well understood, and it is straightforward, if time-consuming, to compute the flow of radiation if the full three-dimensional distribution of gases, aerosols, and clouds is known. In many circumstances, the horizontally averaged results of the three-dimensional calculation can be approximated quite well by a set of one-dimensional calculations performed on each column of the cloud field, ignoring the net transfer of radiation between columns (Cahalan et al. 1994). We call the difference between the full calculation and this so-called independent column approximation (ICA; Cahalan et al. 1994) the 3D effect. The 3D effect is a residual flow; it may be thought of as the component of the radiation field that can not be captured by one-dimensional calculations. The effect is largest in the shortwave where multiple scattering is the most important radiative transfer process. Because the effect is not realized in the natural world, its size can only be assessed through simulations. Nonetheless, the magnitude of the flow is of interest both to modelers, who would like to quantify the errors caused by the ICA (Chambers et al. 1997; Barker et al. 1999; Fu et al. 2000; Benner and Evans 2001; Di Giuseppe and Tompkins 2003), and to observationalists, who would like to understand the circumstances under which measurements of cloud structure and radiative transfer calculations can be compared to (closed with) direct measurements of radiation (Zuidema et al. 2003; McFarlane and Evans 2004). Because the 3D effect depends on every detail of cloud structure, characterizing the effect in a

* Current affiliation: National Center for Atmospheric Research, Boulder, Colorado.

Corresponding author address: Robert Pincus, NOAA–CIRES Climate Diagnostics Center, 325 Broadway, R/CDC1, Boulder, CO 80305.
E-mail: Robert.Pincus@colorado.edu

general way requires calculations for an enormous number of cloud states.

How can realistic, representative sets of cloud distributions be obtained? One attractive possibility is to use ground-based profiling suites, such as those operated by the Atmospheric Radiation Measurement Program (ARM; see Ackerman and Stokes 2003), which combine measurements from ranging active remote sensors (lidars and cloud radars) and passive instruments to provide a long-term, high-frequency time series of the profile of cloud properties above a single location. These profiles are usually interpreted as spatially dependent cloud fields by invoking the frozen turbulence assumption (e.g., Zuidema and Evans 1998), and using an advection velocity to interpret a series of time–height profiles as two-dimensional slices, from which the 3D effect can be computed.

Estimating the 3D effect from a time series of one-dimensional profiles in this way has at least three potential pitfalls. First, the limits of applicability of the frozen turbulence assumption are not known. Profiling instruments observe both advection and temporal evolution of the clouds, and the frozen turbulence assumption explicitly discounts the latter. In addition, in all but the simplest situations, wind speed and direction vary with time and height, making it hard to know what advection velocity is most appropriate. Second, profiling instruments sample only a very small part of the atmosphere. At best, a time series of profiles represents a very small subset of the time-varying instantaneous three-dimensional cloud fields in nature, and the representativeness of this sample (which depends on the cloud field itself) at any given time scale is unknown. Finally, horizontal transports are less important in two-dimensional clouds than in three-dimensional clouds since the edges that affect the transport are more frequent in the latter. Thus, even if the frozen turbulence holds and sampling is sufficient, it is possible that estimates of the 3D effect based on two-dimensional cloud fields will always be biased because they ignore variability in the third dimension.

Here we assess the degree to which 3D radiative transfer effects can be estimated in fields of small cumulus clouds from time series obtained by profiling instruments. We simulate the development of shallow cumulus over the course of a several hours and extract from the simulation a set of profiles of cloud properties as would be obtained by a perfect profiling instrument. We then use Monte Carlo radiative transfer calculations to compute the 3D effect in the complete cloud fields and in various subsets of these fields, including those representing the profiles. The differences between these calculations allow us to assess how accurately the 3D effect may be estimated from a time series of profiles and to disentangle how much of the error is introduced by dimensionality, sampling, and the frozen turbulence assumption.

2. Two views of clouds

a. Simulating evolving cloud fields

We simulate the development of shallow cumulus clouds using a large-eddy simulation (LES) developed by Bjorn Stevens at the University of California, Los Angeles (Stevens et al. 1999, 2001). We focus on shallow cumulus because the 3D effect is likely to be larger in these clouds than in stratiform clouds such as stratocumulus or cirrus. In our experiments the model is configured with grid spacings of 50 m in the horizontal and 40 m in the vertical. The domain extends 8 km horizontally in each direction and from the surface to 4.36 km. Boundary conditions in the horizontal are periodic. Clouds form and dissipate through condensation and evaporation alone: microphysical processes leading to precipitation are not accounted for in our runs, but in these shallow clouds precipitation is unlikely.

The model is initialized with small random perturbations in the potential temperature field. We make three sets of runs, each with a different velocity profile for the applied large-scale wind. In "constant wind" runs, the wind blows from the west at 5 m s^{-1} throughout the domain. In "speed shear" runs, wind direction is constant but velocity increases from 3.5 m s^{-1} near the surface to 7.8 m s^{-1} at the top of the model; the region in which most clouds develop has a mean large-scale wind speed near 5 m s^{-1}. In "directional shear" runs, the applied wind speed is held fixed at 5 m s^{-1} but the direction varies from westerly near the ground to southerly at the top of the domain. The various wind profiles are meant to produce a range of cloud shapes, although our radiative results are not particularly sensitive to which profile is used.

The model is run for up to 12 h at a time, with clouds forming in most simulations during the fifth hour. Surface fluxes of latent and sensible heat, along with advective tendencies for temperature and water, are prescribed based on observations obtained around a continental site in June (Brown et al. 2002). Three-dimensional fields of the atmospheric state, including cloud liquid water content, are saved every five minutes once clouds have begun to form. We simulate observations by a perfect set of profiling instruments by recording the state of the central column in the domain every 10 s. We create different cloud field realizations by varying the initial potential temperature perturbations and running the model again. Our final dataset comprises about 210 h of cloud evolution, divided roughly evenly among the three wind velocity profiles. During most simulations, cloud fraction is relatively low (22 $\pm$ 6% on average) and clouds are only a few hundred meters deep.

b. Constructing two-dimensional scenes from a time series of profiles

We simulate observations by a perfect instrument by extracting the cloud properties in the cloud model's

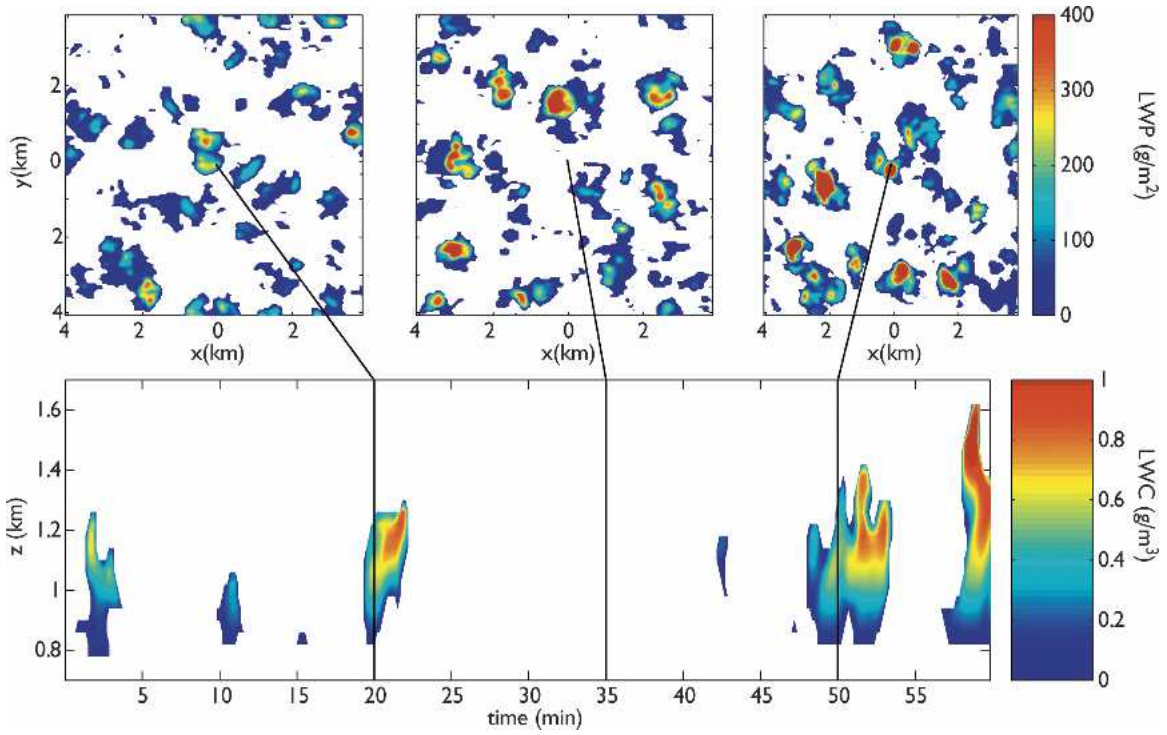

FIG. 1. Two views of a three-dimensional, time-varying field of shallow cumulus clouds simulated by a large-eddy simulation. (top) The horizontal distribution of the column-integrated liquid water path at 3 times over the course of an hour. (bottom) The time–height cross section of liquid water content that would be obtained by a perfect profiling instrument placed at the center of the domain making observations every 10 s.

central column every 10 s. We interpret these time series as two-dimensional slices of cloudiness by choosing a constant advection velocity v_a, and assigning a spatial width of $\Delta x = v_a \Delta t$ to profiles separated by time intervals Δt. We call these cross sections "soda straws," to indicate that they have been constructed from individual columns. These cross sections can be accumulated over any time interval; here we look at windows of 30 min, 1 h, and 3 h.

The same question arises for us as for those using real observations in this way: What value of v_a provides the best mapping from time to space? Here we compute an average wind speed $\bar{v}$ for each time interval by averaging over the cloudy part of the domain at each level and each time step. We assume that $\bar{v}$ equals the advection speed v_a, and ignore the effects of varying wind direction, even in those runs with directional shear in the applied winds. The conversion from time to space (i.e., the horizontal width assigned to each profile) is constant for a given time interval (now interpreted as a 2D scene) but varies between intervals. An example of this process is illustrated in Fig. 1, which juxtaposes three snapshots of an evolving field of shallow cumulus clouds with the time–height cross section of clouds that would be obtained by a perfect profiling instrument operating for an hour.

During the particular hour illustrated in Fig. 1, clouds in the soda straws are more frequent (33.6% versus 28.1%) and substantially thicker (mean liquid water path 39.0 versus 16.9 g m^{-2}) than in the full domain. These differences in cloud properties arise because the profiler samples a very small part of the total domain. The magnitude of the error varies from scene to scene and depends on the length of time over which the soda straws are accumulated. Figure 2 shows the probability distribution functions (PDFs) of cloud fraction and liquid water path in the time-averaged three-dimensional scenes and in those constructed from time series of profiles for time intervals of 30 min, 1 h, and 3 h. Sampling errors make the distributions inferred from the profiler substantially wider than those that include the complete cloud fields. Ensemble mean cloud fraction and liquid water path derived from the soda straws are very accurate, indicating that over very long times the virtual profilers sample the domain more or less completely, but the variability in the model domain is much smaller than would be expected in real observations since the domain is small and the boundary conditions are periodic. The distributions, however, are quite different from those obtained from the full cloud fields, so we expect instantaneous errors in estimates of the 3D effect.

The distributions of cloud physical properties come into closer agreement as the accumulation time increases, which implies that the additional sampling

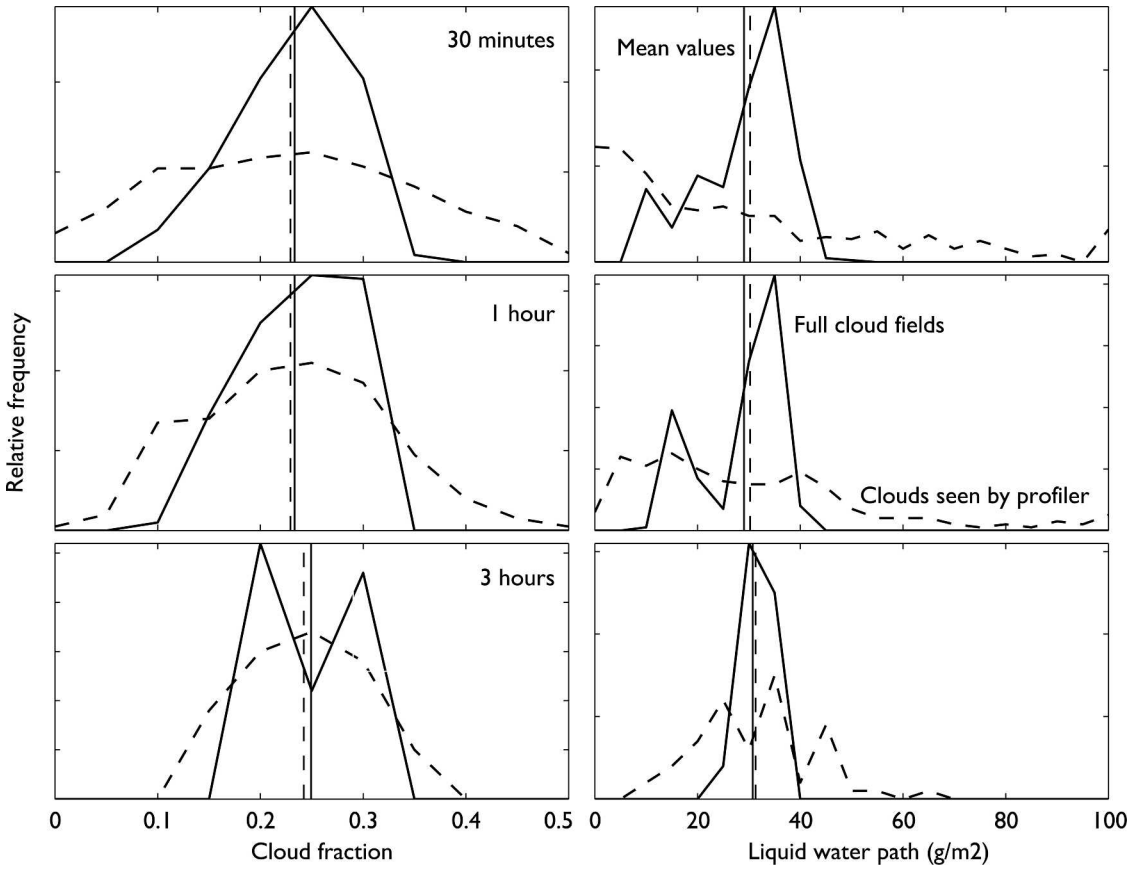

FIG. 2. Probability distribution functions of cloud fraction and mean liquid water path for 3D scenes (solid lines) and for simulated profiler observations (dashed lines) accumulated over 30-min, 1-h, and 3-h intervals. Vertical lines indicate the mean value. The distribution of cloud physical properties inferred from the simulated profiler observations appears to be converging to the truth for long time intervals, but differs substantially at shorter intervals.

achieved over longer times more then compensates for the variability introduced by temporal evolution. But, because the clouds evolve with time, the observations are not statistically stationary. This is why the mean values of liquid water path and cloud fraction are different in the 3-h averages than in the 30- and 60-min averages: the 3-h windows are taken from cloudy hours 1–3 and 4–6 of each simulation, and clouds are more prevalent in the second window, which causes the two peaks in the distribution of 3-h cloud fraction. Furthermore, the 3-h windows do not encompass the entire dataset, so the means are slightly different than for the 30- and 60-min intervals. Note that Fig. 2 is constructed from a set of simulations in which the clouds are known to be very similar; this implies that real measurements taken from a single point will require substantially more averaging to converge toward area averages.

3. Estimates of the 3D flux effect in three-dimensional fields and two-dimensional profiles

The neglect of horizontal transports can affect the calculation of radiation fields throughout the atmosphere. Here we consider domain-averaged broadband shortwave fluxes at the surface, so we are estimating a specific quantity that might properly be called the 3D surface flux effect, though we will continue to refer to it as the 3D effect. We choose broadband surface fluxes so that our results have some relevance to climate problems and to flux closure studies.

We assess the magnitude of the 3D effect in each scene by computing domain-averaged surface fluxes twice, once using the complete three-dimensional radiative transfer F^{3D}, and once using the ICA F^{ICA}. The 3D effect Δ is the difference between these calculations:

$$\Delta \equiv F^{ICA} - F^{3D}. \quad (1)$$

The clouds in these simulations are shallow and not particularly numerous, so their effect on the radiation budget is relative small (50–70 W m^{-2}, depending on the sun angle). We therefore also define a quantity $\tilde{\Delta}$ in which the 3D effect is normalized by the impact of the clouds

$$\tilde{\Delta} \equiv (F^{ICA} - F^{3D})/(F^{clear} - F^{3D}). \quad (2)$$

a. Simulating radiative fluxes in inhomogeneous clouds

We make ICA and three-dimensional radiative transfer calculations using a single Monte Carlo model. This model's performance has been validated by comparison with three others (Barker et al. 2003), though the current version of the code has been made more accurate by integrating cloud optical properties over wavelength within each spectral band. We compute broadband fluxes by integrating over 13 bands in the spectral range 0.26 to 12.2 μm weighted according the incoming solar flux. Cloud optical properties within each LES grid cell are determined from cloud liquid water content by assuming a constant drop number concentration of 200 cm^{-3} and a gamma droplet size distribution with an effective variance of 0.1. Cloud single scattering properties (extinction, single scattering albedo, and scattering phase function) are tabulated for each spectral band using Mie theory. Gaseous absorption is treated using the k distribution from the shortwave version of the rapid radiative transfer model (Mlawer and Clough 1996; Mlawer et al. 1997) using mixing ratio profiles extending from the surface to 40 km. The surface is a Lambertian reflector with the spectral albedo of green grass. The code uses the maximal cross-section method (Marchuk 1980) using a different value of maximum extinction in each of three separate layers (above, below, and in the cloud levels). We use 10^6 photons for each scene, which yields flux accuracies of about 0.3% in homogeneous clouds, and presumably greater accuracy in domain-averaged fluxes when cloud fraction is small. We make calculations for each of seven fixed solar zenith angles equally from 0° (overhead sun) to 75°. We also compute a daytime average in which the photons are introduced at various solar zenith angles according the flux that arrives over the course of a day on which the sun passes overhead at noon. The azimuth is defined such that 0° traverses the variability in the 2D cloud fields.

b. The magnitude of the 3D flux effect in three-dimensional clouds and in soda straws

The upper panels of Fig. 3 show the mean magnitude of the 3D effect as a function of solar zenith angle obtained by averaging over all 3D scenes (Δ_{3D}, shown as solid line) and obtained from soda scenes constructed in 1-h intervals ($\Delta_{\text{soda straws}}$, dashed line). The effect reaches 20–25 W m^{-2} when the sun is very high or very low in the sky. In the lower panels the effect is normalized according to (2) (i.e., we show $\tilde{\Delta}_{3D}$ and $\tilde{\Delta}_{\text{soda straws}}$). In the left-hand panels the clouds have been illuminated uniformly with respect to azimuth; in the right-hand columns all the incoming photons have been introduced at an azimuth of 0° so that the incoming beam encounters the maximum possible variability. The daytime average 3D effect is indicated with a horizontal line.

The impact of the 3D effect on surface and top-of-atmosphere fluxes depends on sun angle (e.g., Welch and Wielicki 1984). When the sun is high, photons that, in a one-dimensional calculation, might undergo many collisions and eventually turn around may instead escape from the edge of clouds, increasing transmission and decreasing reflection (Davis and Marshak 2002). When the sun is low in the sky, on the other hand, photons may enter the clouds from their sides. Under these circumstances photons lower in the cloud need to change direction only slightly to begin traveling upward so that transmission is decreased and reflection increased in three-dimensional clouds relative to their plane-parallel counterparts.

All estimates of the 3D effect in Fig. 3 show this behavior, but the differences between the estimates depend on how the clouds are illuminated. When photons are introduced uniformly in azimuth the absolute value of the 3D effect is smaller in the soda straws at both high and low solar illumination angles. When the illumination is in the plane in which the clouds are variable, though, the 3D effect is underestimated when the sun is high but becomes more accurate as the solar zenith angle increases. This suggests that estimates of the 3D effect are dominated by the number of cloud sides visible to the incoming solar beam; we return to this idea in the next section. The daytime-average 3D effect computed from 3D clouds is small and positive regardless of solar azimuth angle, while the estimates derived from the soda straws are even smaller for random illumination but substantially larger when the soda straw clouds are illuminated from their sides.

We assess the overall error in the estimate of the 3D effect made from a time series of profiles by subtracting the 3D effect estimated from the 3D, time-evolving scenes (i.e., the truth) during some time interval from the 3D effect inferred from the soda straws accumulated over the same time; that is,

$$E_{\text{total}} = \Delta_{\text{soda straws}} - \Delta_{3D}, \tag{3}$$

with $\tilde{E}_{\text{total}}$ defined similarly. The dotted lines in Fig. 3 shows E_{total} and $\tilde{E}_{\text{total}}$, averaged over all 1-h intervals, as a function of solar zenith angle.

c. Why are estimates of the 3D effect made from 2D scenes incorrect?

In section 1 we identified three contributions to E_{total}: insufficient sampling, reliance on the frozen turbulence assumption, and fundamental differences between radiative transfer in two and three dimensions. We assess the importance of each of these effects by computing the magnitude of the 3D effect in a series of scenes, each of which moves a single step closer to the complete assessment using time-evolving 3D fields. In addition to the 3D effect inferred from the simulated observations ($\Delta_{\text{soda straws}}$) and the "true" 3D effect (Δ_{3D}), we also compute the 3D effect as inferred from

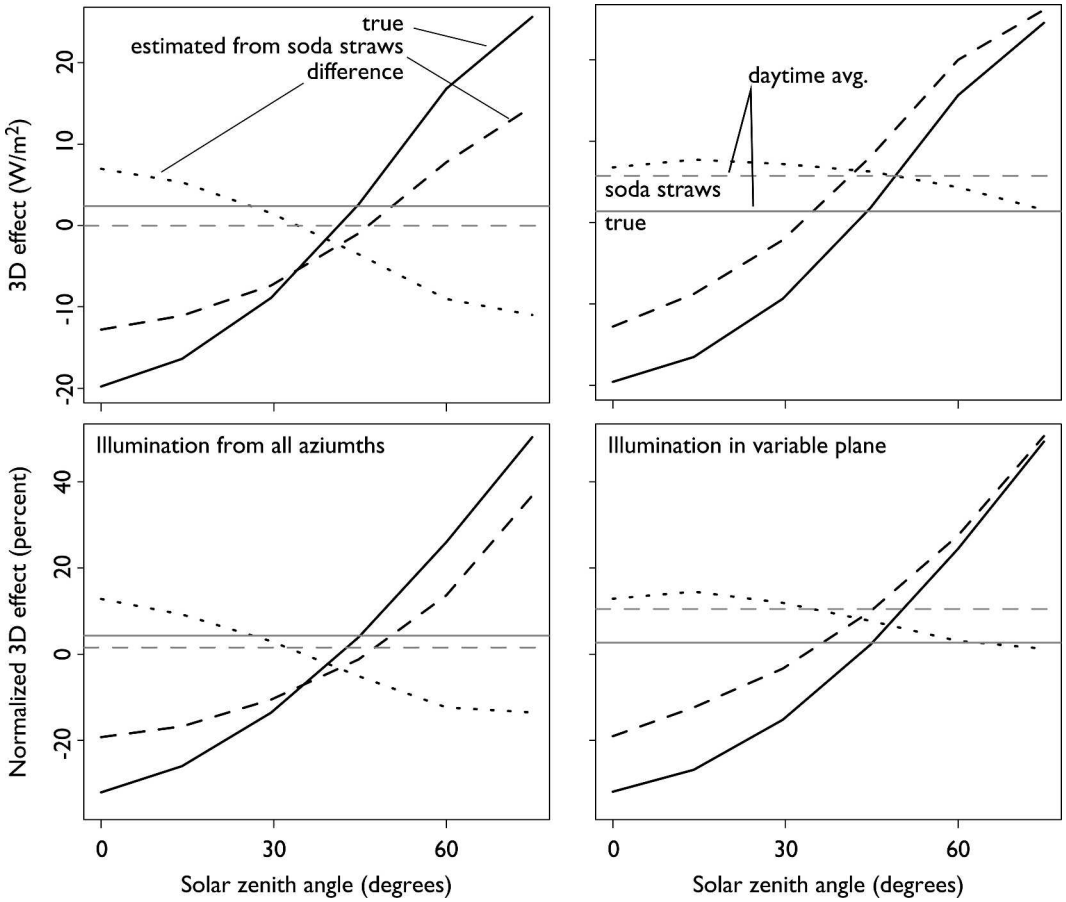

FIG. 3. Dependence of the mean 3D effect on surface fluxes inferred from a set of 3D snapshots (solid lines), from a time series of columns obtained at one location (dashed lines), and the difference between them (dotted lines) as a function of solar zenith angle. (upper) The absolute value of the effect and (lower) the value after it has been normalized by the radiative effect of the clouds themselves, which varies with solar zenith angle. The effect is calculated in 1-h intervals. The time series of profiles is converted to a 2D slice using an advection velocity. The 3D effect reduces transmission when the sun is high and increases transmission when the sun is low. The magnitude of this effect is substantially smaller in the 2D soda straw cloud fields (left) when photons are introduced uniformly at all azimuths. (right) When photons are introduced in the plane of variability, however, the magnitude of the 3D effect is underestimated in the soda straws when the sun is high but becomes more accurate as the solar zenith angle increases.

the single central x–z slice from each 3D scene ($\Delta_{\text{2D-one}}$), as well as the average 3D effect computed across all the x–z slices in each 3D field ($\Delta_{\text{2D-all}}$). The difference between the 3D effect computed in pairs of these fields allows us to assess the magnitude of each contribution to the total error.

1) FROZEN TURBULENCE

Clouds move and change over time, so when we use reconstructed 2D scenes from a time series of profiles we map any temporal changes onto spatial variability. To remove this mapping in our simulations we must find a set of scenes with the same (or nearly the same) limited sampling density and restricted dimensionality as the soda straws but without the soda straws' temporal variability. We choose the single x–z slice through the center of each 3D domain, and use these to compute $\Delta_{\text{2D-one}}$. The error due to the frozen turbulence assumption can therefore be calculated as

$$E_{\text{frozen turb.}} = \Delta_{\text{soda straws}} - \Delta_{\text{2D-one}}. \quad (4)$$

2) SAMPLING

Profiling instruments see a tiny proportion of the clouds around them. To determine how this limited sampling affects estimates of the 3D effect we compare the magnitude of the 3D effect computed in a limited sample ($\Delta_{\text{2D-one}}$, which does not rely on the frozen turbulence assumption) with those computed from all available columns, treated as a set of x–z slices to restrict the radiative transfer to two dimensions:

$$E_{\text{sampling}} = \Delta_{\text{2D-one}} - \Delta_{\text{2D-all}}. \quad (5)$$

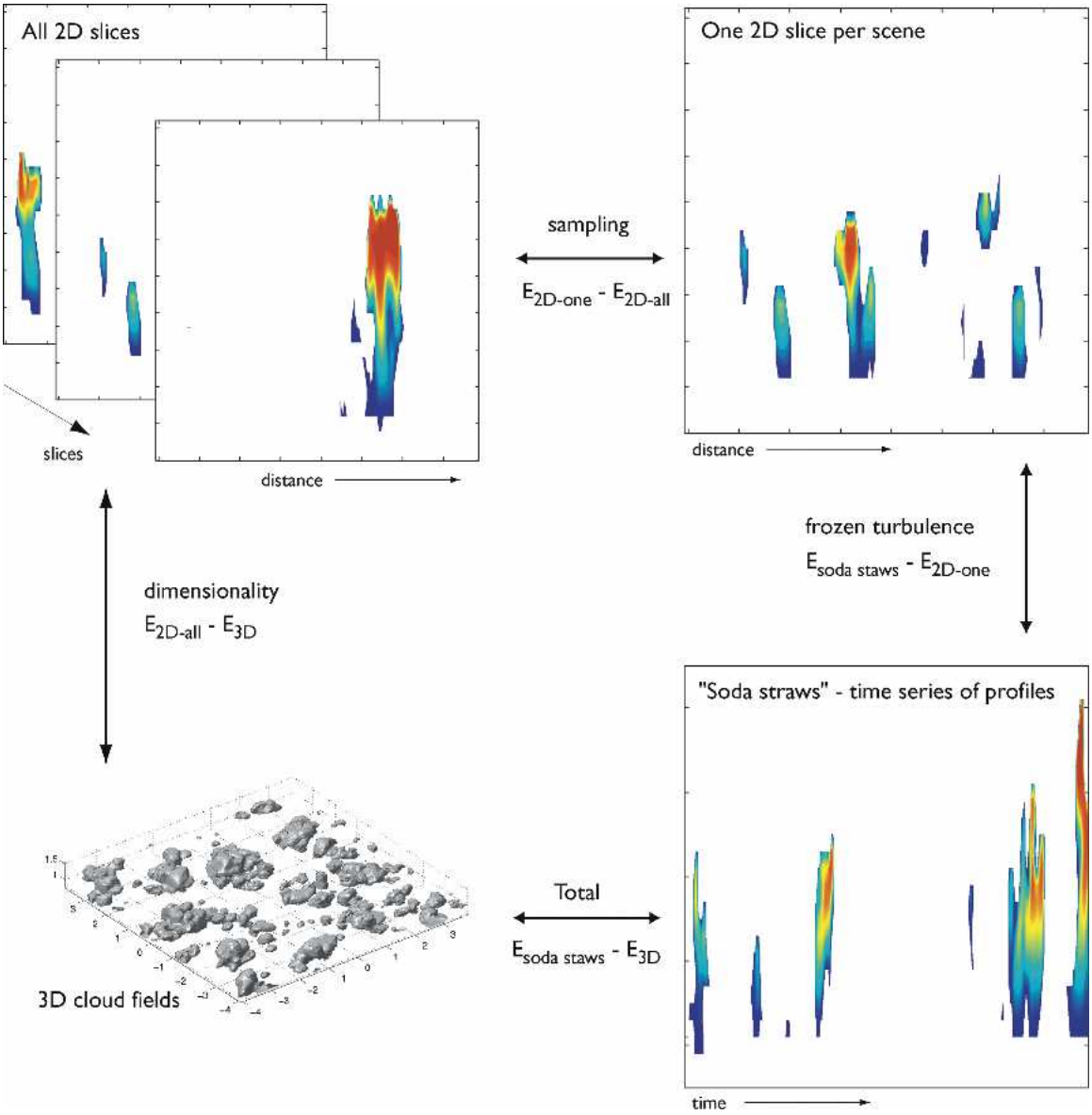

FIG. 4. Decomposition of the total error in estimate of the 3D effect into its constituents. The total error in estimates of the 3D effect in the soda straws can be decomposed into the contributions due to the 2D (as opposed to 3D) nature of clouds in the soda straws, the small sample observed by a ground-based profiling instrument, and the impact of the frozen turbulence assumption. Each source of error can be identified by comparing two estimates of the 3D effect made in cloud fields that differ in one important way. Dimensionality, for example, can be assessed by comparing the 3D effect in the full cloud field with the magnitude of the effect when the cloud fields are treated as a set of 2D slices. The text contains further details.

3) TWO-DIMENSIONAL RADIATIVE TRANSFER

The 3D effect arises precisely because clouds are finite. When cloud structure is known in only two dimensions (as in the soda straws or single slices from the 3D domain) the third dimension is usually assumed to be uniform so that the clouds look like very long sets of railroad ties. This reduces the number of cloud edges that drive the 3D effect, so the 3D effect is typically smaller in 2D clouds than in 3D clouds. We can assess the importance of dimensionality by comparing the 3D effect obtained from the complete set of columns using 2D and 3D radiative transfer; that is,

$$E_{2D} = \Delta_{2D\text{-all}} - \Delta_{3D}. \tag{6}$$

The overall error in estimates of the 3D effect derived from the soda straws described by (3) can now be rewritten as the sum of these components:

$$E_{\text{total}} = E_{\text{frozen turb.}} + E_{\text{sampling}} + E_{2D}. \tag{7}$$

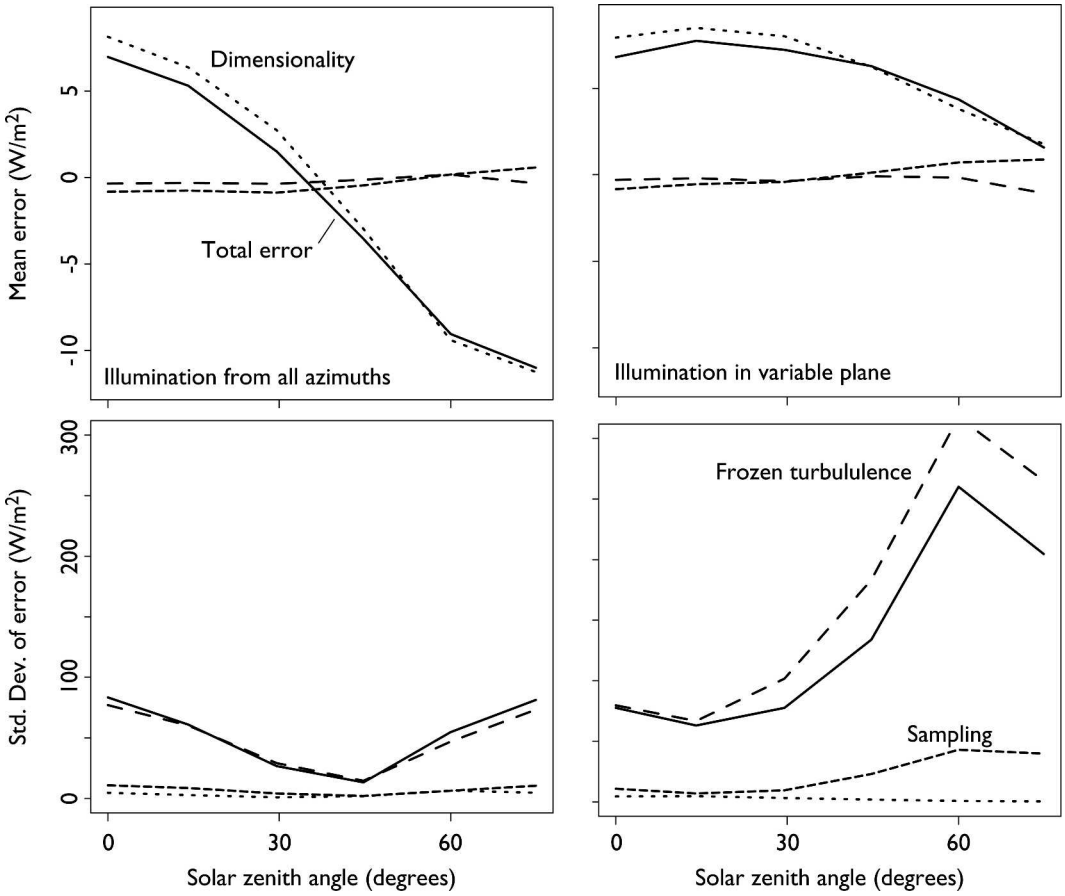

FIG. 5. Contribution to total errors in estimates of the 3D effect in the soda straws (solid line) due to the frozen turbulence assumption (long dashes), limited sampling (short dashes), and the two-dimensionality of scenes reconstructed from a time series of profiles (dots). (upper) The contribution to the mean error; (lower) the contribution to the standard deviation with 210 1-h intervals. As in Fig. 3, (left) results when the clouds have been illuminated from all sides and (right) photons have been introduced in the plane in which the 2D clouds are variable. In all circumstances two-dimensionality dominates the mean error. The impact of frozen turbulence is computed from two small samples of the larger domain, and so causes the largest differences between hours.

The relationships between Eqs. (4)–(7) are illustrated in Fig. 4. Some of these terms on the right-hand side of (7) are expected to contribute random noise to estimates of E_{total}, and others to add to the mean error. To the extent that clouds are uniformly distributed throughout the domain, so that the central slice is a random sample of the entire cloud field, we expect E_{sampling} to be random between scenes with zero mean bias. The change from 2D to 3D radiative transfer, on the other hand, is systematic because it increases the likelihood that the radiation will encounter a cloud edge and so contribute to the 3D effect; this implies that E_{2D} will have a nonzero mean contribution to the total error. The impact of the frozen turbulence assumption is more complicated. The soda straws use the assumption to trade sampling density in space for density in time, which will introduce noise but no mean error if the cloud fields are statistically stationary in time. The assumption also affects cloud morphology in the soda straws, and the distorted shapes will change the surface fluxes computed using 3D radiative transfer, though it's not clear if these changes will introduce a systematic error. We do expect estimates of $\Delta_{\text{2D-one}}$ and $\Delta_{\text{soda straws}}$ for individual hours to vary substantially, though, since both are made from small, but different, subsets of the entire cloud field.

The contribution of $E_{\text{frozen turb}}$, E_{sampling}, and E_{2D} to the mean and variance of the total error E_{total} is illustrated in Fig. 5 for 1-h time intervals. As in Fig. 3, we show results for clouds illuminated from all sides (left column) and from those illuminated in the plane in which the clouds vary (right column). In both circumstances the mean total error is dominated by lack of knowledge about cloud structure in the third dimension (i.e., E_{2D} is the largest contribution). For random illumination the two-dimensionality acts to reduce the magnitude of the 3D effect at all solar zenith angles, while for illumination in the plane of the clouds the

effect is largest when the sun is high and decreases as the solar zenith angle increases.

These results make it clear that estimates of the 3D effect made in two-dimensional clouds are primarily limited by the lack of information about cloud variability in the third dimension (the direction perpendicular to the advection direction). When the sun is high, the 3D effect increases transmission (the effect is negative, as in Fig. 3) because light can escape from cloud edges. Two-dimensional clouds have fewer edges relative to their volume than do three-dimensional clouds, so the magnitude of the 3D effect is reduced (the error is positive). The illumination azimuth is not important when the sun is high since the horizontal component of each photon's propagation is small. When the sun is low, on the other hand, the 3D effect decreases transmission because photons can enter cloud sides and change direction enough to escape from the cloud top. Photons introduced in the plane of the clouds (at azimuth 0) illuminate the cloud sides, so the 3D effect is estimated fairly well. But photons that enter perpendicular to the cloud variability can not encounter cloud sides, so the 3D effect is underestimated. (We highlight this point in Fig. 6, which shows the mean error in estimates of the 3D effect when the clouds are illuminated from all directions, as well as at azimuths of 0° and 90°.) Uniform illumination mixes these scenarios, so the 3D effect is underestimated (the effect is positive, so the error is negative in Fig. 5).

Limited sampling introduces a small amount of variability into hour-by-hour differences between estimates of the 3D effect, as well as a small mean error. Nearly all the interhour variability, however, arises from the frozen turbulence assumption. This is an artifact of the small samples used to calculate the impact of frozen turbulence, and not due to the cloud shapes inferred in the soda straws: we find that frozen turbulence also dominates the difference (not shown) between fluxes computed in soda straws and the complete cloud fields using only the ICA. Results for 30-min and 3-h intervals (not shown) are consistent with Fig. 5: the mean errors do not depend on the averaging interval, while the standard deviation changes with time interval as if each observation were independent (i.e., as the inverse square root of the number of observations in each interval).

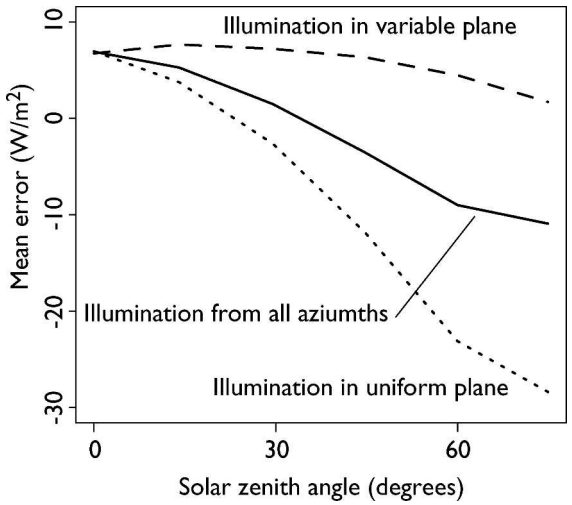

FIG. 6. Dependence of the error in estimates of the 3D effect on solar zenith and azimuth angles. Cloud side illumination becomes a greater part of the overall 3D effect as solar zenith angle increases. This can be captured using 2D clouds if the clouds are illuminated in the place of variability, but clouds illuminated across their variability appear plane parallel, and so the 3D effect is underestimated. Random illumination mixes these two scenarios.

4. Implications

We have used fine scale simulations of cumulus convection and a radiative transfer model to assess how accurately the 3D effect in broadband shortwave surface fluxes can be estimated from measurements made by a ground-based profiler. The 3D effect is negative (3D radiative transfer shows more transmission than ICA) when the sun is high and positive when the sun is low, and in these clouds can be as large as 25 W m^{-2}. When these clouds are illuminated by fluxes at solar zenith angles corresponding to a daytime average, the mean 3D effect is about 2.4 W m^{-2}. This value could be substantially larger if the cloud fields developed preferentially over the course of the day: if clouds were more prevalent at noon, for example, the 3D effect would be larger and negative.

The 3D effect is underestimated when cloud structure is inferred from a time series of columns, as would be obtained by a perfect profiling instrument like a cloud radar. The error arises mostly because clouds with structure in two dimensions have fewer edges relative to their bulk than do clouds that vary in three dimensions. The error could be termed "reasonable," in that the value of the 3D effect inferred from the soda straws is accurate to with about 35% of its true value and the sign of the mean error is known. More accurate measures of the effect might be obtained by using statistical methods to generate stochastic 3D cloud fields from cloud structure statistics obtained from profiles (Evans and Wiscombe 2005).

Estimates of the cloud physical properties and of the 3D effect made for individual time intervals are subject to sampling noise. For hourly intervals, noise in the 3D effect in these clouds ranges from 7% to 20%, depending on solar zenith angle, while for mean liquid water path it reaches about 60%. To reduce the noise in either of these calculations to a few percent requires many tens or hundreds of hours. But these clouds are deliberately constructed to be similar (statistically stationary when taken as an ensemble). That luxury is not available to observationalists. Clouds in the atmosphere do

not remain statistically identical for nearly this long, so accurate estimates of the 3D effect will require compositing observations taken at different times. This, in turn, will require some method for determining how to sort observations into cloud types, and the accuracy of any estimates of the 3D effect will depend greatly on how well this segregation can be done.

Acknowledgments. We are grateful to Bjorn Stevens for providing us with his large-eddy simulation and to Laura Hinkelman for getting us going. We appreciate very helpful comments made by Alexander Marshak and Viktor Venema. This research was supported by the Office of Science (BER), U.S. Department of Energy Grant DE-FG02-03ER63561 and Interagency Agreement DE-AI02-95ER61961.

REFERENCES

Ackerman, T. P., and G. M. Stokes, 2003: The Atmospheric Radiation Measurement program. *Phys. Today,* **56,** 38–44.

Barker, H. W., G. L. Stephens, and Q. Fu, 1999: The sensitivity of domain-averaged solar fluxes to assumptions about cloud geometry. *Quart. J. Roy. Meteor. Soc.,* **125,** 2127–2152.

——, and Coauthors, 2003: Assessing 1D atmospheric solar radiative transfer models: Interpretation and handling of unresolved clouds. *J. Climate,* **16,** 2676–2699.

Benner, T. C., and K. F. Evans, 2001: Three-dimensional solar radiative transfer in small tropical cumulus fields derived from high-resolution imagery. *J. Geophys. Res.,* **106,** 14 975–14 984.

Brown, A. R., and Coauthors, 2002: Large-eddy simulation of the diurnal cycle of shallow cumulus convection overland. *Quart. J. Roy. Meteor. Soc.,* **128,** 1075–1093.

Cahalan, R. F., W. Ridgway, W. J. Wiscombe, S. Gollmer, and Harshvardhan, 1994: Independent pixel and Monte Carlo estimates of stratocumulus albedo. *J. Atmos. Sci.,* **51,** 3776–3790.

Chambers, L. H., B. A. Wielicki, and K. F. Evans, 1997: Accuracy of the independent pixel approximation for satellite estimates of oceanic boundary layer cloud optical depth. *J. Geophys. Res.,* **102,** 1779–1794.

Davis, A. B., and A. Marshak, 2002: Space–time characteristics of light transmitted through dense clouds: A Green's function analysis. *J. Atmos. Sci.,* **59,** 2713–2727.

Di Giuseppe, F., and A. M. Tompkins, 2003: Effect of spatial organization on solar radiative transfer in three-dimensional idealized stratocumulus cloud fields. *J. Atmos. Sci.,* **60,** 1774–1794.

Evans, K. F., and W. J. Wiscombe, 2005: An algorithm for generating stochastic cloud fields from radar profile statistics. *Atmos. Res.,* **72,** 263–289.

Fu, Q., M. C. Cribb, H. W. Barker, S. K. Krueger, and A. Grossman, 2000: Cloud geometry effects on atmospheric solar absorption. *J. Atmos. Sci.,* **57,** 1156–1168.

Marchuk, G., G. Mikhailov, M. Nazaraliev, R. Darbinjan, B. Kargin, and B. Elepov, 1980: *The Monte Carlo Methods in Atmospheric Optics.* Springer-Verlag, 208 pp.

McFarlane, S. A., and K. F. Evans, 2004: Clouds and shortwave fluxes at Nauru. Part II: Shortwave flux closure. *J. Atmos. Sci.,* **61,** 2602–2615.

Mlawer, E. J., and S. A. Clough, 1996: On the extension of rapid radiative transfer model to the shortwave region. *Proc. Sixth Atmospheric Radiation Measurement (ARM) Science Team Meeting,* San Antonio, TX, Department of Energy, 223–226.

——, S. J. Taubman, P. D. Brown, M. J. Iacono, and S. A. Clough, 1997: Radiative transfer for inhomogeneous atmospheres: RRTM, a validated correlated-k model for the longwave. *J. Geophys. Res.,* **102,** 16 663–16 682.

Stevens, B., C. H. Moeng, and P. P. Sullivan, 1999: Large-eddy simulations of radiatively driven convection: Sensitivities to the representation of small scales. *J. Atmos. Sci.,* **56,** 3963–3984.

——, and Coauthors, 2001: Simulations of trade wind cumuli under a strong inversion. *J. Atmos. Sci.,* **58,** 1870–1891.

Welch, R. M., and B. A. Wielicki, 1984: Stratocumulus cloud field reflected fluxes: The effect of cloud shape. *J. Atmos. Sci.,* **41,** 3085–3103.

Zuidema, P., and K. F. Evans, 1998: On the validity of the independent pixel approximation for boundary layer clouds observed during ASTEX. *J. Geophys. Res.,* **103,** 6059–6074.

——, R. Davies, and C. Moroney, 2003: On the angular radiance closure of tropical cumulus congestus clouds observed by the Multiangle Imaging Spectroradiometer. *J. Geophys. Res.,* **108,** 4626, doi:10.1029/2003JD003401.